Effect of antimony on characteristics of $HgBa_2CaCu_{2-x}Sb_xO_{8+\delta}$ superconducting

M. Radhi Jobayr[a,*], S. H. Mahdi[b], E. M. T. Salman[b], K. A. Jasim[b]
aDept. Radiology Techniques /College of Health and Medical Technology / Middle Technical University (MTU), Iraq
bDepartment of Physics, College of Education for Pure Science (Ibn-AL-Haitham)/University of Baghdad, Iraq

In this work, $HgBa_2CaCu_{2-x}Sb_xO_{8+\delta}$ compounds with (x = 0.2, 0.4, 0.6 and 0.8) have been prepared by the solid-state reaction method. Structural, morphological, and electrical properties were investigated using X-ray diffraction (XRD) and scanning electron microscope (SEM) techniques. Using the 4-probe technique to study the effect of antimony-substitution for Copper on the electrical properties of $HgBa_2CaCu_{2-x}Sb_xO_{8+\delta}$ (Hg-1212) phase was investigated by measuring the resistivity as a function of temperature. Results indicate that the addition of antimony (Sb) increases the volume fraction of the phase and changes the superconducting transition temperature Tc of the superconductor to a normal state. The dielectric loss factor and ac conductivity have been investigated at room temperature. It was found that dielectric properties decreased with increasing electric field frequency. It was observed that the best value was 0.8 of the Sb content. Generally, with increasing antimony content, at lower frequencies, higher dielectric criteria are achieved, while at higher frequencies, lower dielectric criteria are achieved. On the other hand, the dissipation of the energy in the dielectric is directly proportional to the dielectric loss factor. Considering this, the increase in the values of ac conductivity is increasing with an increased frequency range to 5 MHz.

1. Introduction

It is well known that the materials and chemical elements vary in their amount of dielectric and, consequently, vary in their conductivity, or resistance, to the electrical current. Superconducting materials show unique capabilities and fascinating intrinsic properties and are very important to the applications of various electronic devices, which require cooling at extremely low temperatures and have been a great choice since the early sixties of the last century [1, 2]. With great scientific development and a growing demand for electronics in most areas of life, it has become necessary to produce different superconductors in an innovative way with superconductivity. For these reasons, serious attempts have been made to produce superconducting conductors at high temperatures [2-5].Also, the properties of the dielectric were studied for various materials to produce superconductors and even to achieve superconductivity at normal temperatures [6-9]. The materials' interaction with the electric fields can be characterized by the dielectric properties of the non-conducting materials. The dissipation of part of the energy when removing the dielectric field and the absorption of electric potential energy and storage in the form of polarization within the dielectric material are important properties [10, 11].The space charge effects in a low-frequency region were attributed to the oxygen ions at high temperatures. Also, the dielectric properties do not show the same behaviors and intrinsic contributions at all frequencies and temperatures, since the conduction mechanisms change greatly for a variety of electronic devices depending on temperature, frequency, and doping concentration and impurities. As a result, it is critical to identify the dielectric properties and electrical conductivity of these materials

and report their behavior with frequency and temperature, which provides valuable information about estimates or predictions of conduction and polarization mechanisms. Generally, of the polarization mechanisms, interfacial and oriental polarizations play pronounced and important roles in calculating dielectric properties. At high frequencies (MHz region), the dielectric constant can become almost saturated at all temperatures. Whereas the interfacial polarization mechanism is very sensitive to the range of low frequencies starting from a kHz to a few kHz because the mechanism of this polarization occurs as a physical barrier presence, impeding the migration of charge carriers [12-14]. However, since the discovery of the first high-temperature superconductors based on mercury $HgBa_2CuO_{4+x}$ (Hg–1201) material with a high critical transition temperature (Tc = 98K), extensive research on superconductivity has been conducted with promising results. Despite the great success in the field of superconductivity, many of the grand challenges of superconductivity are still related to superconducting materials. These challenges include the difficulty of forming these materials in the form of wires or circuits so that they can carry high currents that are not allowed in normal conductors, which has been a fundamental issue since the discovery of superconductivity [16–18]. This system is one of the systems belonging to the family of superconducting mercury compounds called HBCCO [19].

Superconducting materials show great promise in high-voltage and high-performance electronic applications. The discovery of high-temperature superconducting ceramic compounds (HTSC) ignited the first spark of a new revolution in materials research and industrial applications. It is worth mentioning that study into element substitution or addition methods and procedures can give and open up new paths for understanding the mechanisms by which superconductivity occurs in elements and compounds, particularly those based on the composition of copper oxide (Cuprates) [20–22]. Despite these benefits, their application has not been as prevalent as that of other HTSC materials. This is owing to the extreme difficulty of synthesizing HTSC phases containing Hg, notably the Hg-Base family, due to their extreme vulnerability to contamination by moisture and carbon dioxide. After synthesis, Hg-Base samples are known to deteriorate quickly. As a result, considerable effort has lately been made to increase the stability of the HTSC Hg-Base stages. It is currently known that Pb+4 or Tl+3 partial substitution of HgOd in the hypoxic HgOd layer can stabilize the structure of Hg-1223 and raise the Tc of produced samples [20, 23, 24]. Furthermore, partial substitution of Hg by Sb+4 or Re improves the chemical stability and flow stabilization capabilities of Hg-1223 [21-23]. Despite numerous researches on substitution and addition, no specific methodologies and mechanisms have been found in the addition and replacement of elements in this type of material, complementing our scientific project of studying the replacement of chemical elements in superconducting compounds.

In this work, in order to meet the major challenges in meeting the high conductivity requirements at normal temperature, the role of antimony partial substitution of the superconducting compound ($HgBa_2Ca_1Cu_{2-x}Sb_xO_{8+\delta}$), its effects on structural characterization (structure and surface morphology pattern), and thermal properties (resistivity versus temperature). We also investigate the influence of antimony content on the dielectric properties of $HgBa_2Ca_1Cu_{2-x}Sb_xO_{8+\delta}$ at room temperature in different concentrations of antimony to replace copper and their characterization.

2. Materials and methods

Samples were prepared with compositions of $HgBa_2Ca_1Cu_{2-x}Sb_xO_{8+\delta}$ (where x = 0.0, 0.2, 0.4, 0.6, and 0.8) directly from high-purity (99.99%) oxide compounds of HgO, BaO, CuO, CaO, and Sb2O3 with purity (98.95%) by a single step of the solid state reaction method, and mixed according to their molecular weights as shown in Table (1).

Table 1. Weights for pure powders.

Oxides	Molecular weights
HgO	[200.59+15.999]
BaO	2* [137.33+15.999]
CaO	[40.078+15.999]
CuO	(2-x) * [63.546+15.999]
Sb_2O_3	x[(2*121.76)+ (3*15.999)]

Using a grey agate mortar to maintain the purity of the samples, the powders were thoroughly mixed and then sieved using a fine sieve (13.5 mm). Resistance versus temperature of the samples was measured using a 4-point probe technique with a cooling nitrogen chamber equipped with a digital temperature controller (Thermocouple, type-K). The four-point probe method finds wide usage in the material industry, including metals, for the purpose of measurement of conductivity due to its high accuracy and few stages of sample preparation. This technology consists of four terminals (sensors). Two of these probes are used to source current, and the other two probes are used to measure voltage, a nano-ampere meter, a nano-voltmeter, and a DC current source. For the measurement procedure, the samples were configured into tablets for resistivity measurements with a diameter of 1.5 cm and a thickness of about 0.3 cm by using a hydraulic press with a high-pressure of up to 70 MPa. The samples used for resistivity measurements were connected to copper leads using silver paint. Finally, we can preview the possible effect of Sb-doping on the physical properties by the current (I) being passed through the sample, resulting in a potential difference (V) that appears across this sample. The sample resistance is given by the relationship, $\rho = V.A/I.L$, where $A = \pi r^2$ is sample area, r is diameter of the sample and L is the distance between two probes ($L = 29.272 \times 10^{-6} m$) [25]. To minimize mercury loss during the reaction, the tablets were wrapped in silver paper. Hg-1212 samples were created in a one-temperature furnace using an oxide mixture. The obtained data reveal that a short synthesis time at a rather low temperature (t = 5h and T = 840 °C) yields almost no formation of the Hg-1212 phase at all, while prolongation of t up to 10 hours leads to some increase in Hg-1212 content. This fact indicates that the desired reaction of Hg-1212 formation is hindered at low temperatures, for instance, kinetically, and therefore longer annealing times are necessary. Then samples were inserted into an established furnace. The furnace was gradually heated at a rate of 5°C per minute to 850°C and it was kept at this temperature for 24 hours. To avoid the possible effects of any change in sintering time and cooling rate on phase purity, superconducting transition temperature, and electrical resistance, the samples were cooled slowly to room temperature. After this stage, the obtained compound is of a hard nature and black in color. X-ray diffraction (XRD) pattern measurements were done on the annealed samples using (Shimadzu7000 XRD, Cu kα) over the 2θ range from 20° to 70°. The surface morphological photographs were recorded using the Scanning Electron Microscope (SEM, JSM-5300, JEOL, Japan). After the sample configuration, the amplitude and loss of latency were examined directly by the LCRmeter at room temperature within the frequency range of 50 Hz to 5 MHz. By using the following Eq. (1), the real and imaginary parts of the dielectric constant and the alternating electrical conductivity are calculated as [10, 11, 15].

$$\varepsilon' = d * C/A * \varepsilon_o \tag{1}$$

ε' is the real dielectric constant, is the sample thickness, A is the area surface of the specimen, C is the capacitance of the sample, and P is the Permittivity of Free Space. Dielectric loss tangent (tan δ) is defined as follows:

$$tan\delta = \varepsilon''/\varepsilon' \tag{2}$$

$$\varepsilon'' = tan\delta * \varepsilon' \tag{3}$$

where ε'' is dielectricdispassion factor.

$$\sigma_{a.c} = 2\pi f \varepsilon_o \varepsilon'' \tag{4}$$

$\sigma_{a.c}$is alternating electrical conductivity, and f is frequency. Complex impedance spectroscopy (CIS) has been shown to be a one-of-a-kind, adaptable, and successful approach for interpreting various dynamical features of electrical transport processes in polycrystalline materials in different frequency bands as a function of temperature. An alternating voltage signal can be delivered to the material to measure matching current responses. While CIS is most commonly utilized in polycrystalline materials, it is also used to investigate the link between electrical and structural features and their total contribution to sample conductivity [25, 26]. In general, the frequency-dependent behavior of materials in complex impedance spectroscopy can be represented in any of the following basic formalisms: complex impedance (Z^*), complex electric modulus (M^*), complex permittivity (ε^*), and tangent loss (tan $\boldsymbol{\delta}$)), all of which are related [22, 23]: complex impedance: $Z^* = Z' - jZ''$, complex permittivity: $\varepsilon^* = \varepsilon' - j\varepsilon''$ and complex modulus: $M^* = \frac{1}{\varepsilon^*} = M' + jM''$, where Z' ,ε', and $M'$are real parts andZ'', ε'',and M'' are imaginary parts. $Z^*$and $M^*$are the most frequently used representation of complex data. So, the complex impedance (Z^*) is interrelated to the complex electric modulus (M^*) for a simple parallel RC circuit as follows [26-30]:

$$M^* = j\omega C_0 Z^* = \omega C_0 Z'' + j\omega C_0 Z' \tag{5}$$

where $\omega = 2\pi f$ is angular frequency, C_0 is the geometrical capacitance, and $j = \sqrt{-1}$ is the imaginary factor.

3. Results and discussion

XRD patterns of the nominal composition (Hg-1212), $HgBa_2Ca_1Cu_{1.4}Sb_{0.6}O_{8+\delta}$ and $HgBa_2Ca_1Cu_{1.2\ Sb0.8}O_{8+\delta}$ have been shown in Fig. 1–Fig. 3 respectively. Fig. 1 shows the XRD pattern of the main peak (110) of the nominal composition (Hg-1212) sample as a reference pattern. It is observed that the main peak of Sb-doped samples shift towards the right. Detailed structural analysis of samples to determine the lattice-parameters of three samples and to understand the effect of Sb substitution on the Hg-1212 crystalline structure was done using the Rietveld-refinement technique and the MAUD program as a function of the Sb-concentration level. XRD patterns representing the influence of Sb addition on the phase composition of the Hg-1212 samples are marked. The reflections corresponding to the high phases of Hg-1212 (Fig. 1), $HgBa_2Ca_1Cu_{1.4}Sb_{0.6}O_{8+\delta}$ (Fig. 2) and $HgBa_2Ca_1Cu_{1.2\ Sb0.8}O_{8+\delta}$ (Fig. 3) are highlighted. Only the 2θ region between 20 and 70° is shown. As shown in Table 3, the dominant high Tc (T_{offset}) phase (H phase) and a small number of indefinite phases, as well as the effects of Sb content that play a significant role in peak position, shift with increasing Sb content.
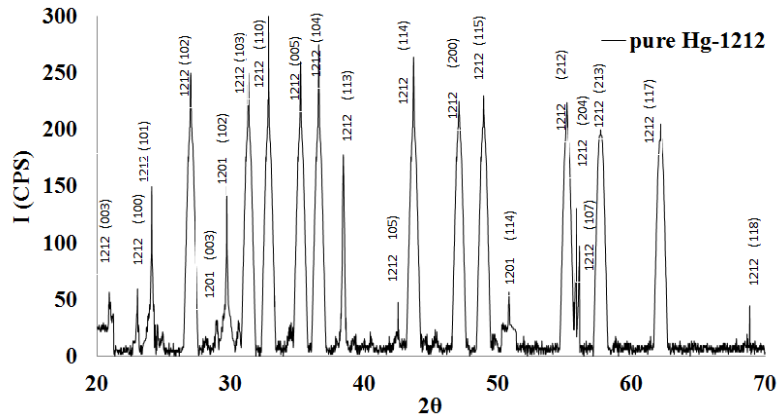

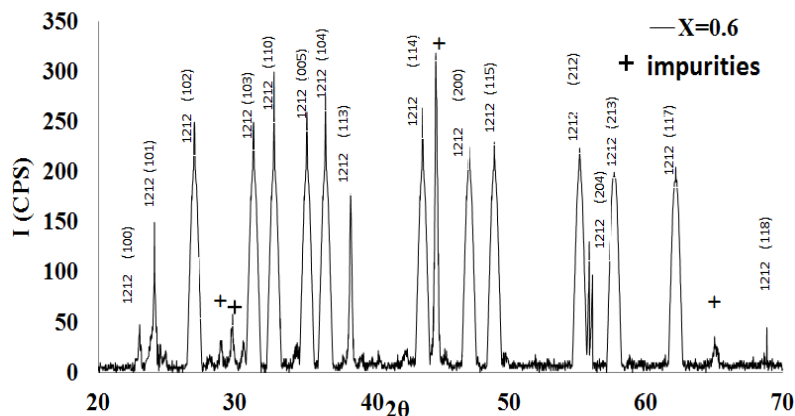*Fig. 1. XRD patterns of nominal composition Hg-1212 sample.*

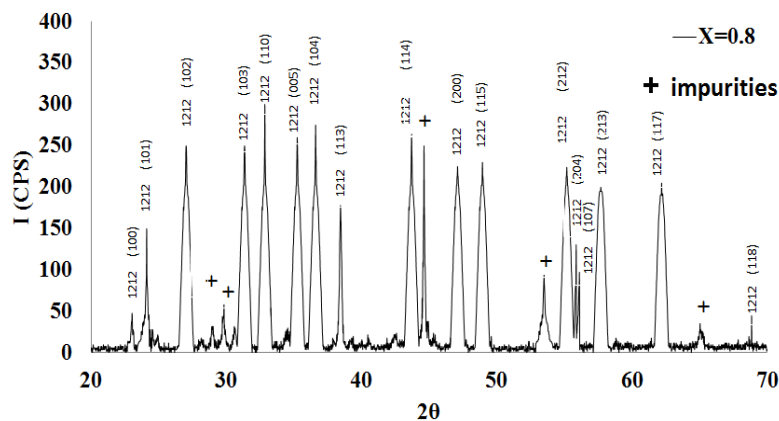Fig. 2. XRD patterns of $HgBa_2Ca_1Cu_{1.4}Sb_{0.6}O_{8+\delta}$sample.

Fig. 3. XRD patterns of $HgBa_2Ca_1Cu_{1.2}Sb_{0.8}O_{8+\delta}$sample.

An explanation is that the high-Tc of cuprate superconductors depends on a crystalline structure similar to that of perovskite structure 20, 28. It is noteworthy that the Hg-based superconducting oxides have a mixed compound of the phase (Hg-1201) with a low critical temperature, which is unstable at high temperatures and causes an unequal reaction to the constituent substances. While the phase (Hg-1212) has a high critical temperature, these phases include several CuO_2 layers. Therefore, the high and low phases can be produced by the solid-state reaction of the phase to form the phase ($HgBa_2CaCu_2O_8$). Then the low-temperature phase will subsequently undergo an equivalent interaction, and as a result of this, the high-temperature phase will grow. High phase germination (Hg-1212) can form if any additional layers of Cu-Ca-O are inserted into the base phase (Hg-1201). XRD patterns show the mechanism of high-phase formation (Hg-1212), which passes through three stages: the inducing period, the accelerating period, and the front-forming period. In the first stage, the phase (Hg-1201) decreases quickly, and in the second stage, it appears that the phase decreasing velocity (Hg-1201) does not become faster but some slows down, so the high phase (Hg-1212) cannot be formed by direct deposition of the phase (Hg-1212) but by the solubility of the phase [21-22]. The formed low phase is moistened by the liquid phase rich in atoms (Ca, Cu), which also contains atoms of the added element (Sb).As for the liquid phase, it forms at the surface of the low phase (Hg-1201), which arises from melting or corrosion partials [23]. On the other hand, the liquid phase containing Sb in abundance can spread spontaneously to the surface of phase Hg-1201 residual, and through an interaction, the (Hg-1212) nuclei form on the interface of the phase [20-24]. After the formation of the (Hg-1212) nuclei, the reaction enters the crystal growth stage. Figures 2 and 3, which represent Sb-ratios of 0.6 and 0.8, respectively, show the appearance of impurities with the high-phase at percentages of 11.81015 for Sb-0.6 and 12.3442 for Sb-0.8. After the formation of the (Hg-1212) nuclei, the reaction enters the crystal growth stage. The phase cohesion is responsible for the change in

resistivity in cooling conditions at Tc, which explains the difference in Tc at concentrations (x = 0.6, x = 0.8). In both Figures 2 and 3, which represent the Sb-ratios of 0.6 and 0.8, respectively, it was observed the appearance of impurities with the high-phase at percentages of 11.81015 for Sb-0.6 and 12.3442 for Sb-0.8.

In Figure 4, the temperature dependent D.C electrical resistivity of $HgBa_2CaCu_{2-x}Sb_xO_{8+\delta}$ compounds with (x = 0, 0.2, 0.4, 0.6, and 0.8) is shown. The temperature dependence of the resistivity function at temperature for $HgBa_2CaCu_{2-x}Sb_xO_{8+\delta}$ compounds with (x = 0, 0.2, 0.4, 0.6, and 0.8) is presented in figure 4. It is observed that the critical temperature Tc is affected due to antimony (Sb) addition. The shapes of the curves below exhibit two different regimes. The first part of the high temperature corresponds to the normal state which shows metallic behavior (above the onset and offset critical temperature Tc). The other part is the region characterized by the contribution of cooper pair fluctuation to conductivity when approaching Tc. This is mainly due to the increased rate of pair formation to lower the temperature. By increasing antimony (Sb) content, the normal state resistivity changes from metal to isolator behavior.

Figure 4 shows that at high temperatures, samples with x = 0 ($HgBa_2CaCu_2O_{8+\delta}$), x = 0.6 ($HgBa_2CaCu_{1.4}Sb_{0.6}O_{8+\delta}$), and x = 0.8 ($HgBa_2CaCu_{1.2}Sb_{0.8}O_{8+\delta}$) exhibit normal state metallic behavior, with the critical transition temperatures at zero resistance $T_{c(off)}$ = 125, 121, and 139 K, and transition temperatures $T_{c(on)}$ = 142, 137, and 146 K, respectively. While the sample x = 0.2 ($HgBa_2CaCu_{1.8}Sb_{0.2}O_{8+\delta}$), the superconducting transition is absent, but in the high temperature region, electrical resistivity shows metal behavior. Samples with x = 0.4 ($HgBa_2CaCu_{1.6}Sb_{0.4}O_{8+\delta}$) show an isolator behavior. The behavior of the sample x = 0.2 is similar to the behavior of insulators, so the electrical resistance was a very small decrease with the decrease in the temperature of the sample, so the superconducting behavior was not obtained due to the change in the crystal structure of the sample and the change in each of the axes of the crystal lattice and the percentage of oxygen in addition to The number of gaps makes the electron pair unable to cross the two Cu-O layers. As for the behavior of the sample x = 0.2, it is similar to the behavior of superconducting materials, so the electrical resistance gradually decreased with the decrease in the temperature of the sample, but we were not able to obtain the transition degrees $T_{c(off)}$ and $T_{c(on)}$ and that is less than the temperature of liquid nitrogen, so we need liquid helium To know both. This is interpreted as these impurities having an auxiliary effect of 1212-phase in obtaining a high-transition at temperature Tc. When compared to the nominal composition of Hg-1212, the pure compound that Tc had equivalent to 125K, the critical temperatures became 133K and 143K, respectively.
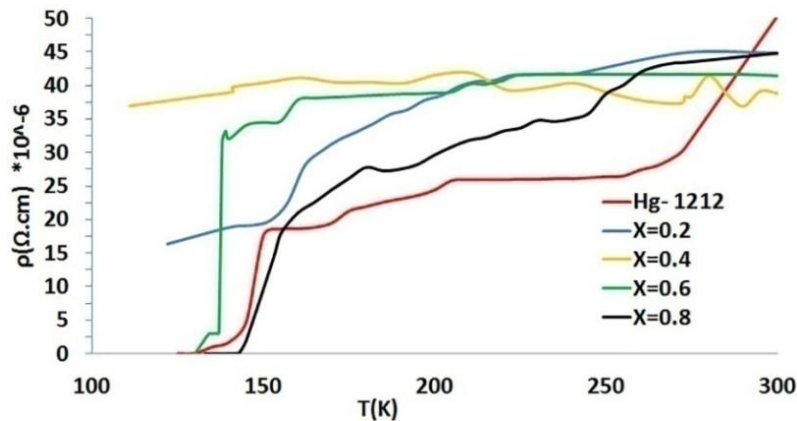

Fig. 4. Temperature dependence of resistivity versus the Sb-contentfor $HgBa_2Ca_1Cu_{2-x}Sb_xO_{8+\delta}$ samples.

Table 2. Superconductivity temperatures of the $HgBa_2Ca_1Cu_{2-x}Sb_xO_{8+\delta}$ samples.

Sample	$T_{onset}(K)$	(T_{offset}) (K)	$\Delta T(K)$
$HgBa_2CaCu_2O_{8+\delta}$	142	125	17
$HgBa_2Ca_1Cu_{1.8}Sb_{0.2}O_{8+\delta}$	-	-	-
$HgBa_2Ca_1Cu_{1.6}Sb_{0.4}O_{8+\delta}$	-	-	-
$HgBa_2Ca_1Cu_{1.4}Sb_{0.6}O_{8+\delta}$	137	121	16
$HgBa_2Ca_1Cu_{1.2}Sb_{0.8}O_{8+\delta}$	146	139	7

This indicates that the electron properties of superconducting materials depend on doping. High-temperature superconductors are electrical insulators and non-magnetic without doping, so when the Sb concentration increases, these compounds become minerals. Superconductivity arises when the concentration of the grafted material (Sb) is large and this is shown by the results in Table 3.

It can be seen that lattice parameters and Packing Fraction (c/a) compositions for the samples with x=0.6 ($a \approx 3.1401\text{Å}$, $c \approx 12.8062\text{Å}$ and $c/a \approx 4.078278$) are close to those with x =0.8 ($a \approx 3.1716\text{Å}$, $c \approx 12.8947\text{Å}$ and $c/a \approx 4.065677$) as shown in Table 3.

Table 3. Calculated lattice parameters compositions for (x= 0.0, 0.6, and 0.8).

Sample x value	a	c	c/a	High phase (Hg-1212) %	Low phase (Hg-1201) %	Impurities %	T_C (K)	Eg (eV) at 0 (K°)
nominal composition Hg-1212	3.0515	12.7214	4.168901	92.6397	7.36024	-	125	0.03805
$HgBa_2Ca_1Cu_{1.4}Sb_{0.6}O_{8+\delta}$	3.1401	12.8062	4.078278	88.1898	-	11.81015	133	0.03958
$HgBa_2Ca_1Cu_{1.2}Sb_{0.8}O_{8+\delta}$	3.1716	12.8947	4.065677	87.6557	-	12.34420	143	0.04049

Also, this study showed that the dielectric constant at room temperature changes according to the frequency of the electric field voltage and the substitution between Cu and Sb as follows: Fig. 5 shows that the real electrical dielectric frequency decreases when the frequency of the charged electric field is increased. This linear decrease is due to the fact that the molecules of the material consist of positive and negative charges. The center of negative charges is often applied to the center of positive charges of these molecules. In fact, the influence of an external electric field can be understood by the fact that the positive and negative charges are separated by a small distance in the molecule under the influence of this field. The positive charges are driven by the field in a given direction, while the negative charges of these molecules move in the opposite direction. As a result, the positive and negative charge centers do not match, and the dipole is thus formed. Thus, a molecule can be said to be polarized [17].
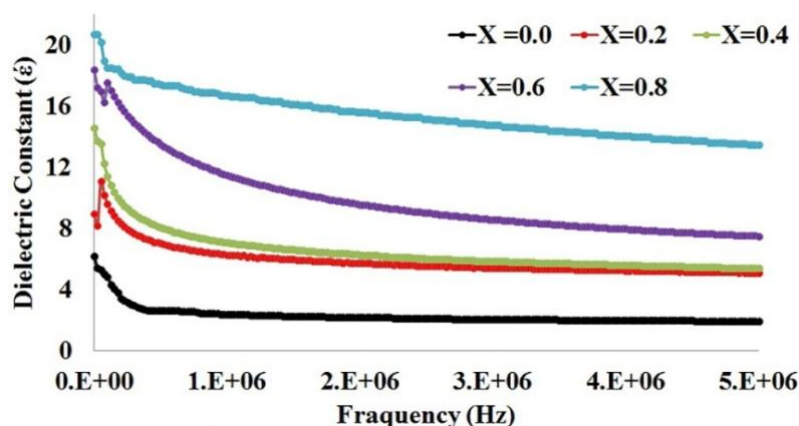
Fig. 5. Variation of real dielectric dispassion factor of HgBa₂Ca₁Cu₂₋ₓSbₓO₈₊δversus frequencies
at different Sb contents.

As for the effect of Sb substitution instead of Cu, the results of this study, as shown in Fig.6, show that the best value of the dielectric constant at partial compensation of Sb by 0.8 instead of Cu. When increasing the content of Sb, we observe at a low frequency, 50Hz, that the value of the dielectric constant is 6.16 when x = 0 and 20.7 when x = 0.8. But these values decrease by increasing the frequency. For example, at high frequencies of 1 MHz and 5 MHz, the dielectric constants when x = 0 are 2.4 and 1.9, respectively, and 16.7 and 13.4 when x = 0.8. In general, we observe at the low frequencies of 50H that the highest solubility constants are achieved; increasing the Sb content, but we obtain low values of the dielectric constant at high frequencies of 1MHz and 5MH with increased content due to the applied field effect and polarization mechanics [18].
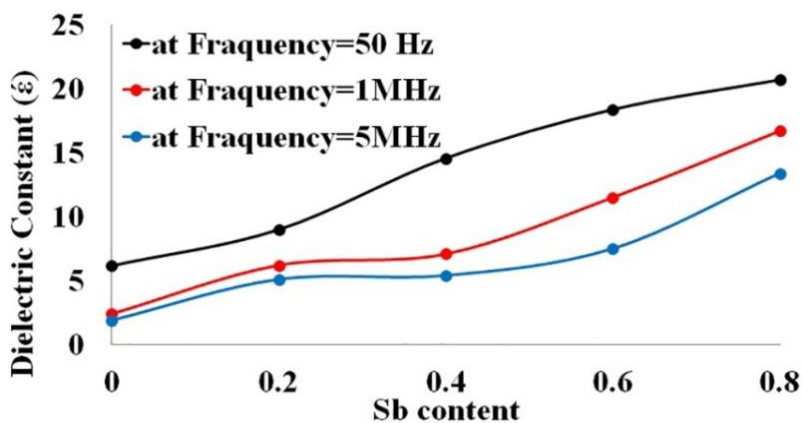

Fig. 6. Variation of real dielectric dispassion factor of HgBa₂Ca₁Cu₂₋ₓSbₓO₈₊δversusSb content
at different frequency.

Fig.7 refers to the decrease of the loss of dielectric with the frequency calculated according to Equation (3).
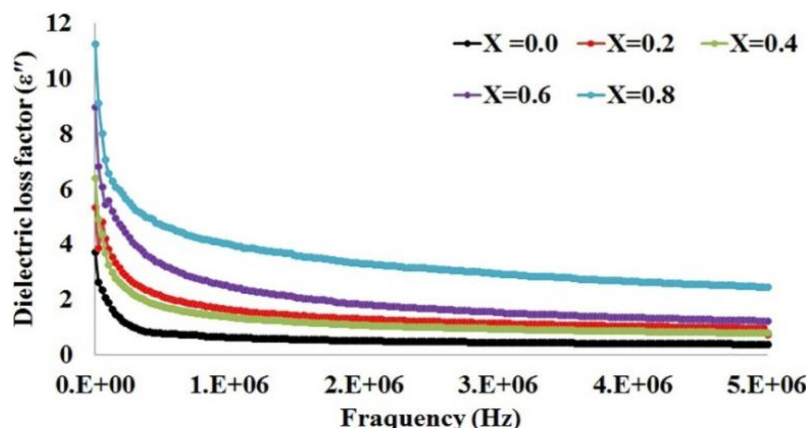
Fig. 7. Variation of the imaginary dielectric dispassion factor of $HgBa_2Ca_1Cu_{2-x}Sb_xO_{8+\delta}$ versus frequencies with different Sb content.

According to equation (3), the results show that the values decrease as the frequency increases. The dissipation of the power in the dielectric is directly proportional to the loss factor electrostatic. Thus, this factor is a major concern for many applications. One of the main advantages of materials that are used as electrical insulators is that the loss factor is too small. The variation of dielectric modulus (M′ and M″) as a function of frequency range (50Hz–5MHz) of samples with x =0.0, 0.2, 0.4, 0.6, and 0.8 at room temperature is shown in Fig. 8 (a–b). M′ and M″ tend to decrease to their minimum values as frequency increases (values of M′ and M″ appear convergent at 50Hz to 5MHz frequencies), while they shift to higher values as Sb content increases (as shown in table 4). The frequency region minimum determines the range in which M′ and M″ are at their highest. The M′ and M″ are confined to minimum values at frequencies of 1MHz and 5MHz, remaining stable in the 1MHz to 5MHz frequency range. With a rise in frequencies, the frequency corresponding to M′ and M″ maximum indicates the presence of the electronic polarization phenomenon [25, 27].

Table 4. Complex modulus (M'andM") in the frequencies50Hz, 1MHz and 5MHz.

| X%	M′	M"	M′	M"	M′	M"
	at F=50Hz		at F=1MHz		at F=5MHz	
0.0	14.3162018	14.25301034	0.989347456	0.70406217	0.677784014	0.259276865
0.2	15.09033217	15.02697032	4.119279645	4.009339915	0.618910207	0.446217127
0.4	41.30601406	41.26761161	1.880723585	1.765834218	0.790488285	0.632402246
0.6	80.95713998	80.92935805	5.951700671	5.882770379	1.711540459	1.596842428
0.8	126.9454896	126.9234701	16.05988024	16.01434257	12.0799154	12.02458495

(a)

(b)
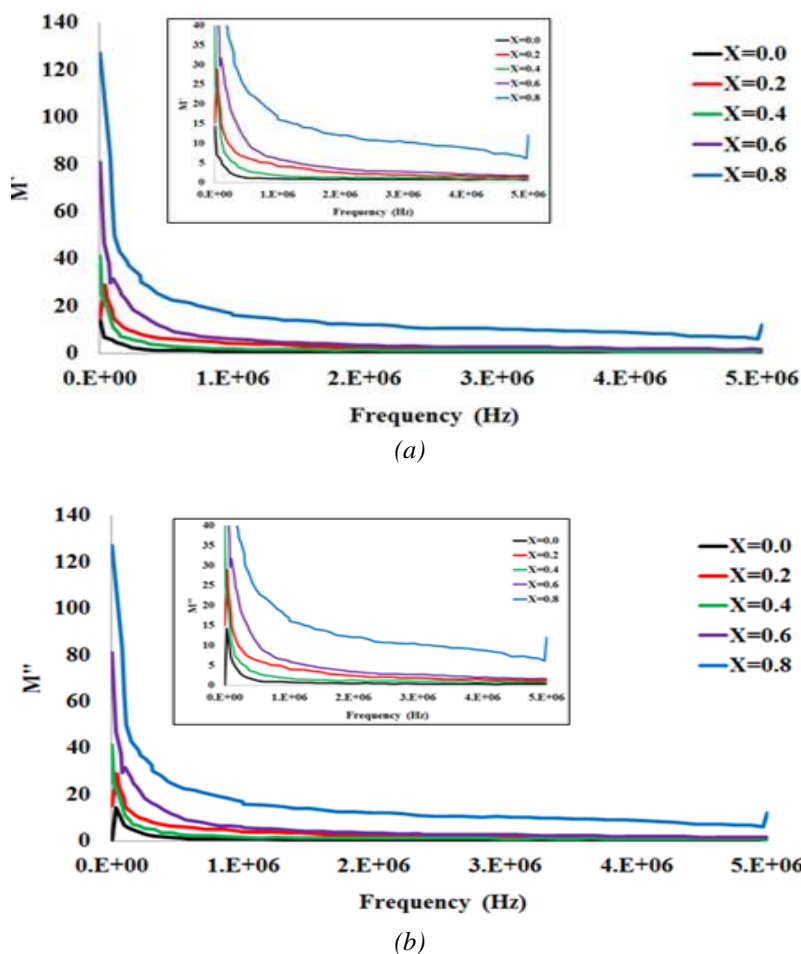
Fig. 8. Complex modulusversus frequency plots measured at room temperatures with different Sb content; (a) real part and (b) imaginary part.

The plot of the real and imaginary portions of impedance (Z and Z") as a function of the frequency of the ac voltage at room temperature is presented in Fig. 9 (a-b). Z′ and Z", which in principle behave the same, it is clear that the curves of the frequency-dependent impedance exhibit maximum distinctive values at lower frequencies. However, they tend to decrease with increasing frequency, showing that ac conductivity increases with increasing frequency. In other words, at high frequencies, the values of Z and Z" trend to the minimum, but at lower frequencies, they tend to the maximum (as shown in table 5), suggesting the presence of an electrode polarization phenomenon in the samples [25, 27]. The curve exhibits a sigmoidal variation at low frequencies, although the saturation region at higher frequencies suggests the mixed nature of electronic, dipolar, and orientation present in the samples.

Table 5. Complex impedance (Z' and Z") in the frequencies50Hz, 1MHz and 5MHz.

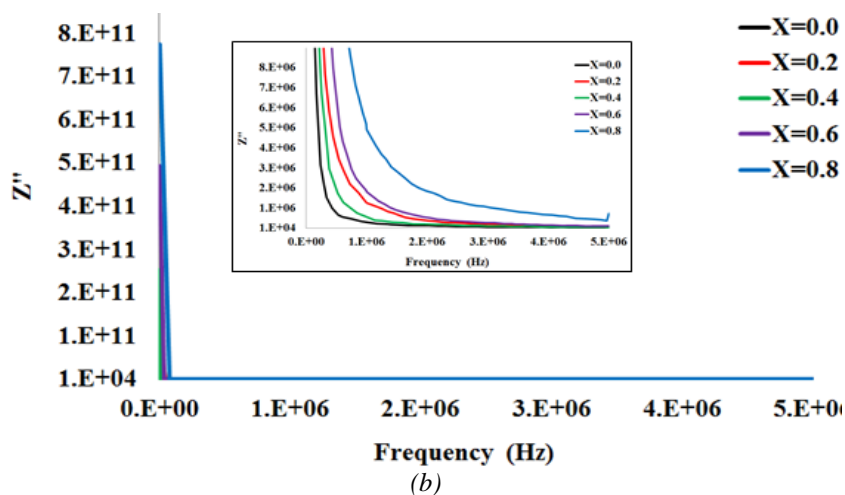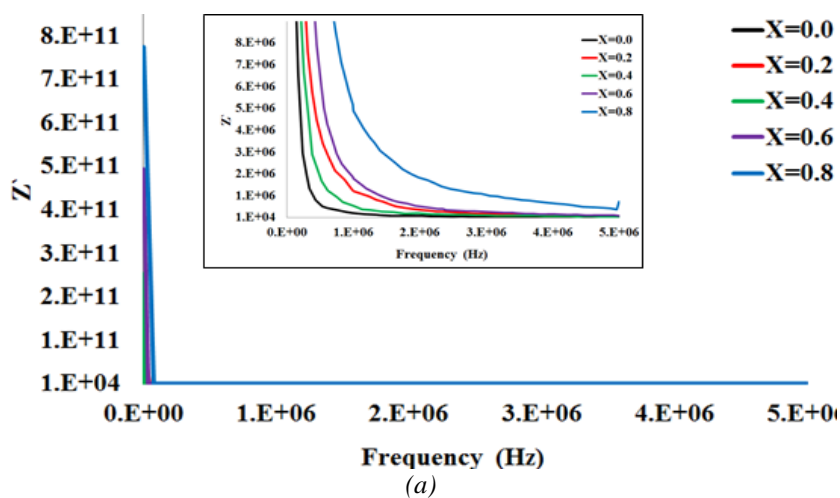| X%	Z′ (Ω)	Z"(Ω)	Z′ (Ω)	Z"(Ω)	Z′ (Ω)	Z"(Ω)
	at F=50Hz		at F=1MHz		at F=5MHz	
0.0	8.71×10^{10}	8.75×10^{10}	2.15×10^{5}	3.02×10^{5}	1.58×10^{4}	4.14×10^{4}
0.2	9.18×10^{10}	9.22×10^{10}	1.23×10^{6}	1.26×10^{6}	2.73×10^{4}	3.78×10^{4}
0.4	2.52×10^{11}	2.52×10^{11}	5.40×10^{5}	5.75×10^{5}	3.87×10^{4}	4.83×10^{4}
0.6	4.95×10^{11}	4.95×10^{11}	1.80×10^{6}	1.82×10^{6}	$9. \times 10^{4}$	1.05×10^{5}
0.8	7.76×10^{11}	7.76×10^{11}	4.89×10^{6}	4.91×10^{6}	7.35×10^{5}	7.38×10^{5}

Fig 9. Complex impedance versus frequency plots taken at room temperatures with different Sb content; (a) real part and (b) Imaginary part.

The maximum absorption limit at the frequency increase is depicted in Fig.10, which reflects the direct relationship between the loss factor (the imaginary constant) and the loss of the tang (tan δ) in equation (2).
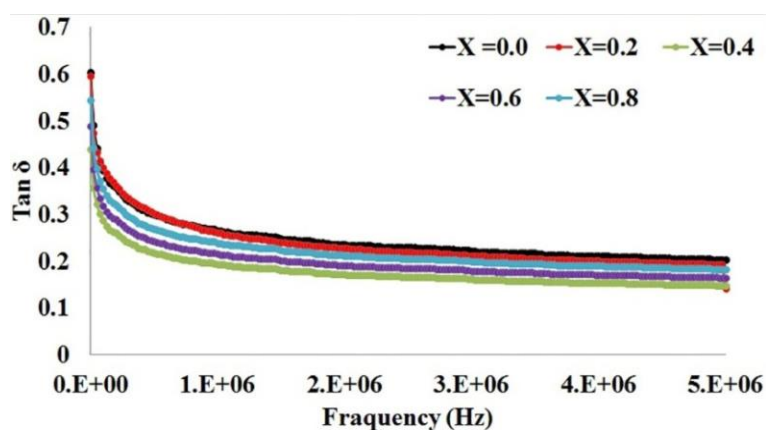

Fig. 10. Variation of Tan δ of $HgBa_2CaCu_{2-x}Sb_xO_{8+\delta}$ versus frequency at different Sb contents.

It is clear from the values of $\sigma_{a.c}$ that it increases as the application frequency increases to 5 MHz. As is seen from Fig. 11, an increase in the applied frequency characteristics has been dependent on the direct relationship between $\sigma_{a.c}$ and frequency as stated in (4), due to the polarization of the charge carriers.
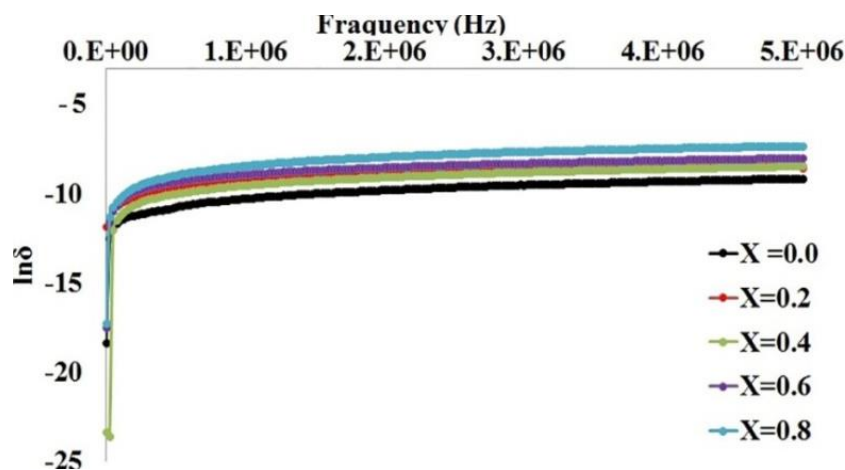

Fig. 11.Variation of alternating electrical conductivity of HgBa$_2$Ca$_1$Cu$_{2-x}$Sb$_x$O$_{8+\delta}$versus frequency at different Sb contents.

Analysis performed by scanning electron microscopy (SEM) revealed that the Sb addition with concentrations (x = 0.2, 0.4, 0.6, 0.8), compared to Sb-free, induced some morphological changes (Fig.12). As shown in the figures (12b and c), the presence of Sb promoted the growth of elongated, well-formed crystallites with a characteristic size of 10–30 μm. The microscopy images of the specimens with x (x = 0.2, x = 0.4) show microscopic structures with fine grains without a preferred direction (randomly directed). As for the models with the content x (x = 0.6 and x = 0.8) figure (12 d, e), the growth of the grains is a regular geometric shape (plate-like crystals) similar to platelets and less porous, and this increases the contact areas effectively. With the increase in the concentration of Sb irregular morphology seen, this could be an aggregation of Sb particles.
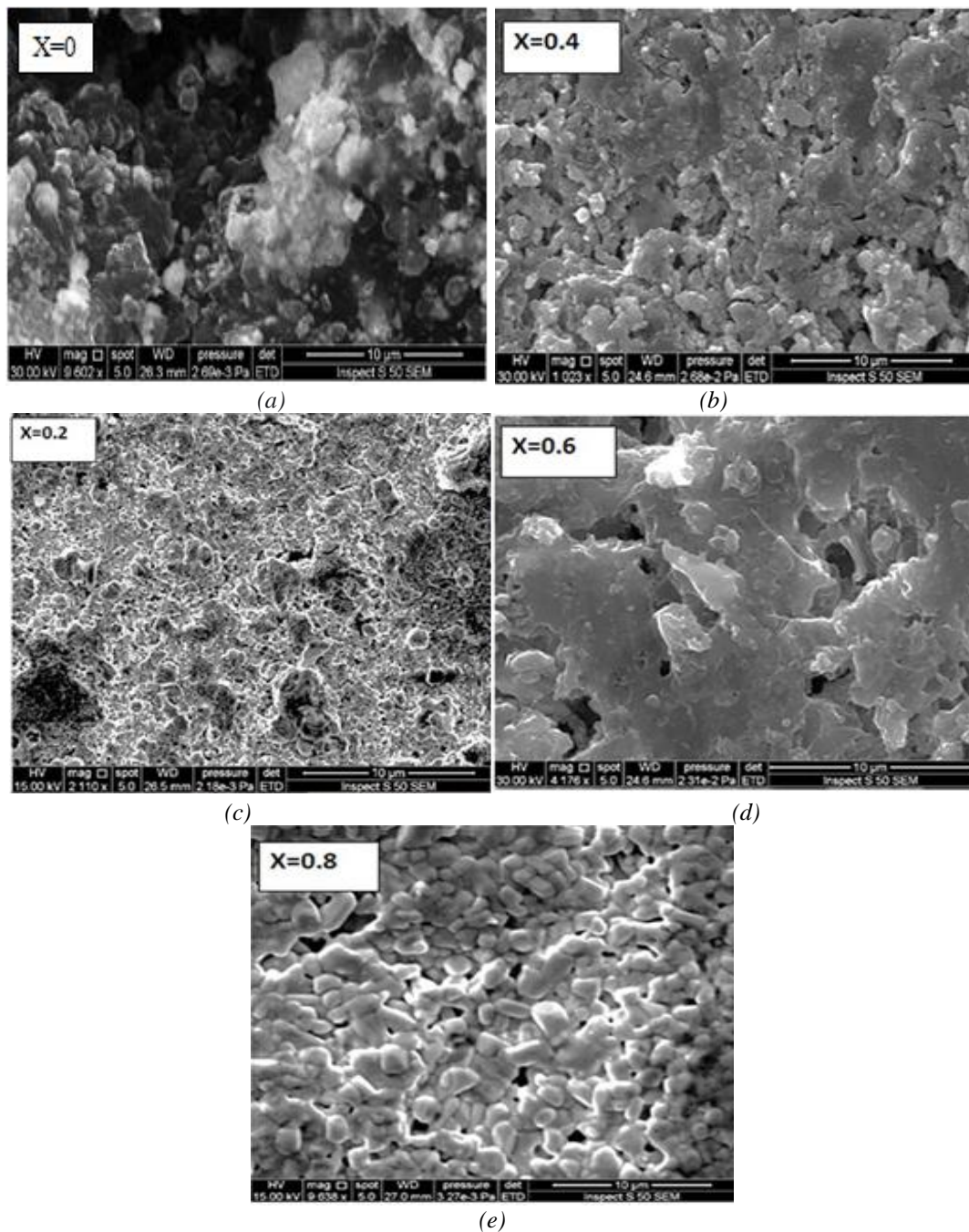
Fig. 12. SEM images of Hg-1212 samples obtained with (a) Sb-free (b) $Cu_{1.8}Sb_{0.2}$ (c) $Cu_{1.6}Sb_{0.4}$ (d) $Cu_{1.4}Sb_{0.6}$ (e) $Cu_{1.2}Sb_{0.8}$.

4. Conclusions

The resistivity measurement indicated that the superconductivity of $HgBa_2Ca_1Cu_{2-x}Sb_xO_{8+\delta}$ with x equal to 0.6 and 0.8 possesses a zero-resistivity transition at 133 K and 143 K, respectively. This contrast implies that the resistive transition is due to Sb-content effect. On the other hand, this study showed that there was a remarkable change in the dielectric constant and dispassion factor (tan δ) commensurate with the variation of both the frequency interval of about 10 Hz to 5 MHz and the substitution between Cu and Sb. Remarkably, the real dielectric constant decreases as the frequency of the electric field increases. Furthermore, the best value for the dielectric constant at compensation is 0.6 of Sb instead of Cu. In general, the dielectric constant is increased by

increasing the Sb content at low frequencies (50Hz or less) and decreasing at high frequencies (1MHz and more).Also, the results indicate that the loss of the dielectric decreases as the frequency applied increases, as the dissipation of the energy in the dielectric is directly proportional to the loss factor of the dielectric. Thus, this factor is a major concern for many applications. One of the main advantages of materials that are used as electrical insulators is that the loss factor is too small.

References

[1] A. Sacco, Rene. Sustain. Ener. Rev., 79 (2017) 814-829; https://doi.org/10.1016/j.rser.2017.05.159

[2] Z. Alborzi, V. Daadmehr, J. Supercond Nov. Magn., 33 (2020) 387-396; https://doi.org/10.1007/s10948-019-05209-2

3. M. I. Khan, K. A. Bhatti, R. Qindeel, N. Alonizan, H. S. Althobaiti, Res. Phys. 7 (2017) 651-655; https://doi.org/10.1016/j.rinp.2016.12.029

4. R. Sultana, P. Rani, A. K. Hafiz, R. Goyal, V. P. S. Awana, J. Supercond Nov. Magn., 29 (2016) 1399-1404

5. B. H. Hussein, S. H. Mahdi, S. A. Makki, B. K. Al-Maiyaly, Ener. Proc., 157 (2019) 100-110; https://doi.org/10.1016/j.egypro.2018.11.169

6. T. A. Al-Dhahir, K. A. Jasim, S. H. Mahdi, J. chem. biol. phys. sci., 4 (2014) 1-8

7. R. N. Fadhil, M. R. Jobayr, A. R. Khazaal, S. H. Mahdi, Ener. Proc., 157 (2019) 626-634; https://doi.org/10.1016/j.egypro.2018.11.228

8. X. Huang, T. Iizuka, P. Jiang, Y. Ohki, T. Tanaka, J. Phys. Chem. C, 116 (2012) 13629-13639; https://doi.org/10.1021/jp3026545

9. S. Devesa, M. P. F. Graça, F. Henry, L. C. Costa, Int. J. Mater. Eng. Innov., 8 (2017) 12-26

10. K. C. V. Rajulu, B. N. Mohanty, Int. J. Eng. Tech., 8 (2016) 51-60; https://doi.org/10.18052/www.scipress.com/IJET.8.51

11. B. Parimala, , J. H. Siddalingappa, N. B. Desai, J. Poly. Comp., 6 (2018) 1-8

12. M. Mumtaz, N. A. Khan, Phys. C: Supercond., 469 (2009) 182-187

13. N. A. Khan, , M. Mumtaz, A. A. Khurram, J. Appl. Phys., 104 (2008) 033916

14. C. C. Wang, G. Z. Liu, M. He, H. B. Lu, Appl. Phys. Lett., 92 (2008) 052905; https://doi.org/10.1063/1.2840195

15. S. N. Putilin, E. V. Antipov, O. Chmaissem, M. Marezio, Nature, 362 (1993) 226-228; https://doi.org/10.1038/362226a0

16. A. Arya, A. L. Sharma, J. Phys. Cond. Matter., 30 (2018)165402; https://doi.org/10.1088/1361-648X/aab466

17. M. R. Jobayr, A. H. A. Al Razak, S. H. Mahdi, R. N. Fadhil, In AIP Conf. Proc., 1968, (2018) 030021

18. S. B. Ocak, A. B. Selçuk, S. B. Bayram, A. Ozbay, J. opto. Adva. Mater. 17 (2015) 1747-1755

19. C. W. Chu, L. Z. Deng, B. Lv, Phys. C Supercond. Appl., 514 (2015) 290-313; https://doi.org/10.1016/j.physc.2015.02.047

20. K. A. Jasim, S. A. Makki, A. Abud Almohsin, Phys. Proc. 1(2014) 336-41

21. K. A. Jasim, J. supercond. Nov. Magn., 26 (2013) 549-552; https://doi.org/10.1007/s10948-012-1787-7

22. A. H. Ali, A. K. D. Ali, K. A. Jasim, In AIP Conf. Proc., AIP Publishing LLC, 2123 (2019) 020079

23. K. A. Jasim, T. J. ALwan, K. H. Mahdi, H. L. Mansour, Turk. J. Phys., 37 (2013) 237-241

24. K. Kishio, J. Shimoyama, A. Yoshikawa, K. Kitazawa, O. Chmaissem, J. D. Jorgensen, J. Low Temp. Phys., 105 (1996) 1359-1365; https://doi.org/10.1007/BF00753889

25. M. K. Shamim, S. Sharma, S. Sinha, E. Nasreen, J. Adva. Diel., 7 (2017) 1750020

26. A. A. Pelmenev, I. B. Bykhalo, I. N. Krushinskaya, R. E. Boltnev, Low Temperature Physics, 45 (2019) 276-281; https://doi.org/10.1063/1.5090040

27. A. K. Behera, N. K. Mohanty, S. K. Satpathy, B. Behera, P. Nayak, Cent. Eur. J. Phys., 12 (2014) 851-861

28. S. K. Barik, R. N. P. Choudhary, A. K. Singh, Adv. Mat. Lett, 2 (2011) 419-424; https://doi.org/10.5185/amlett.2011.2228

29. A. Singh, S. Suri, P. Kumar, B. Kaur, A. K. Thakur, V. Singh, J. Alloy. Comp., 764 (2018) 599-615; https://doi.org/10.1016/j.jallcom.2018.06.071

30. E. Płaczek-Popko, J. Trzmiel, Z. Gumienny, E. Wojtyna, J. Szatkowski, Acta. Phys. Polo. A, 5 (2008) 1279-1283; https://doi.org/10.12693/APhysPolA.114.1279